# Determination of interface preference by observation of linear-to-circular polarization conversion under optical orientation of excitons in type-II GaAs/AlAs superlattices

R. I. Dzhioev
*A. F. Ioffe Physico-Technical Institute, 194021, St. Petersburg, Russia*

H. M. Gibbs
*Optical Sciences Center, University of Arizona, Tucson, Arizona 85721*

E. L. Ivchenko
*A. F. Ioffe Physico-Technical Institute, 194021, St. Petersburg, Russia*

G. Khitrova
*Optical Sciences Center, University of Arizona, Tucson, Arizona 85721*

V. L. Korenev, M. N. Tkachuk, and B. P. Zakharchenya
*A. F. Ioffe Physico-Technical Institute, 194021, St. Petersburg, Russia*
(Received 3 October 1996; revised manuscript received 24 February 1997)

A comprehensive investigation of exciton optical orientation and alignment in type-II GaAs/AlAs(001) superlattices in longitudinal and transverse magnetic fields is presented. We observe the previously predicted type-II orientation-to-alignment conversion induced by a longitudinal field due to the anisotropic exchange splitting of the localized-exciton radiative doublet. A theory of polarized exciton photoluminescence under polarized excitation is developed, that takes into account the fine structure of the excitonic quartet, the exciton spin relaxation, and the difference in the lifetimes of electric-dipole-active and inactive states. By comparing experimental and theoretical curves, the main parameters characterizing the level splitting, the recombination rates, and the spin relaxation of localized excitons are deduced. Field-induced polarization conversion provides an effective method to measure the interface preference, i.e., the difference between the fractions of excitons localized on AlAs/GaAs and GaAs/AlAs interfaces. We have also observed the field-induced transformation from [100] to [110] linear polarization, which is direct evidence of exciton cascade kinetics. [S0163-1829(97)05444-1]

## I. INTRODUCTION

Exciton spin polarization has been extensively studied both in bulk semiconductors[1,2] and semiconductor heterostructures.[3,4] The optical orientation of excitonic spins is a particular case of a more general phenomenon, namely, the selective optical excitation of excitonic sublevels. Another example of the selective excitation is the optical alignment of excitons by linearly polarized radiation. In contrast to the optical orientation, which means the photoinduced inequality in the populations of the states $|m\rangle$ with the exciton spin $m$, say with $m=1$ and $-1$, linearly polarized light can, under resonant conditions, excite the exciton states with a definite direction of oscillating electric-dipole moment. Such a state can also be described as a coherent superposition, $(|1\rangle+e^{i\Phi}|-1\rangle)/\sqrt{2}$, of the states $|\pm 1\rangle$, where the phase $\Phi$ is determined by the orientation of the light polarization plane.

It often happens that the symmetry of the system is reduced because of microscopic or local anisotropy in the plane normal to the light propagation direction, as well as due to application of an external field (magnetic field, uniaxial strain). As a result, the optical orientation and optical alignment are interconnected, and one needs to consider not only circular-circular and linear-linear but also linear-circular and circular-linear configurations of the polarizer and analyzer.

Under steady-state excitation, linear-circular or circular-linear polarization conversion has been observed on localized excitons in GaSe crystals in an oblique magnetic field[5] and in type-I GaAs/$Al_{1-x}Ga_{1-x}$As quantum-well structures in a longitudinal magnetic field.[6] The time-resolved transformation between the linear polarization $P_{l'}=(I_{[100]}-I_{[010]})/(I_{[100]}+I_{[010]})$ in the axes [100] and [010], and the circular polarization $P_c$ was observed in type-II GaAs/AlAs superlattices (SL's) in quantum-beats experiments.[7,8] It was demonstrated experimentally,[9–13] and explained theoretically,[14,15] that for localized heavy-hole excitons $e1$-hh1$(1s)$ in type-II GaAs/AlAs SL's the degeneracy of the radiative doublet $|\pm 1\rangle$ is lifted, and the two split sublevels $E_{[110]}$ and $E_{[1\bar{1}0]}$ are dipole-active, respectively, along the [110] and [110] directions in the interface plane. Moreover, in a single SL with fixed layer thicknesses, there exist two classes of localized-exciton states characterized by the same absolute value but opposite signs of the anisotropic exchange splitting $\hbar\omega_2 \equiv E_{[110]}-E_{[1\bar{1}0]}$. The explanation is based on the fact that excitons contributing to the low-temperature photoluminescence (PL) of the undoped type-II SL's are bound electron-hole pairs localized by the structure imperfections in

 

the plane of interfaces with an $X$ electron and a $\Gamma$ hole confined inside two neighboring AlAs and GaAs layers. According to the theory,[14,15] the two classes of excitonic states with opposite signs of $\omega_2$ are excitons localized at the AlAs-on-GaAs and GaAs-on-AlAs interfaces, i.e., localized excitons with the electron confined in either the right or in the left AlAs layer relative to the GaAs layer in which the hole is photoexcited.

Time-resolved polarization oscillations[7,8] can be instructively compared with space-dependent oscillations in the polarization of the light propagating perpendicularly to the principal axis of a uniaxial birefringent medium. Since in type-II GaAs/AlAs SL's the quantum-beats frequency $\omega_2$ is much higher than the inverse characteristic lifetime $T^{-1}$, the optical orientation and the optical alignment for the incident light polarized along the [100] or [010] axis can hardly be observed in the cw excitation regime. In a longitudinal magnetic field, $\mathbf{B}\|z$, the steady-state optical orientation effect is restored.[11] In addition to the restoration of $P_c$, the theory predicts the appearance of a remarkable linear polarization $P_l=(I_{[110]}-I_{[1\bar{1}0]})/(I_{[110]}+I_{[1\bar{1}0]})$ induced by the magnetic field under excitation with circularly polarized light. Because of the existence of two classes of excitons, the conversion effect is proportional to the imbalance factor $f=(N^{(+)}-N^{(-)})/(N^{(+)}+N^{(-)})$, where $N^{(+)}$ and $N^{(-)}$ are the concentrations of excitons localized at the AlAs-on-GaAs and GaAs-on-AlAs interfaces, respectively. In the experiment reported in Ref. 11 the magnetic-field-induced orientation-to-alignment conversion was not observed, presumably because the densities of states for the two classes of excitons with positive and negative values of $\omega_2$ were accidentally equal to each other. Since technologically the quality of GaAs/AlAs interfaces differs from that of AlAs/GaAs interfaces, the two densities of states are expected to be different as a rule. Thus the aim of the present work was to observe and investigate, both experimentally and theoretically, the magnetic-field-induced conversion between the circular and linear polarizations predicted in Ref. 11, thus proposing an effective method to measure an important structural parameter, namely, the interface preference factor $f$. In Sec. II we develop a theory of optical orientation and alignment of excitons in an external magnetic field, taking into account the fine structure of the $e1$-hh1$(1s)$ level, the exciton spin relaxation, and the difference between lifetimes of optically active and inactive sublevels. In the main text we derive expressions obtained under simplifying assumptions and keep the detailed calculation in Appendix A. In Sec. III we describe the experimental setup. In Sec. IV we present experimental data on the exciton-polarized PL, including the observation of the linear-circular polarization conversion effect under steady-state excitation and determination of the interface preference factor $f$, and compare experiment with theory.

## II. THEORY

The lowest excitonic level $e1$-hh1$(1s)$ consists of four sublevels taking into account the electron ($s_z=\pm\frac{1}{2}$) and heavy-hole ($J_z=\pm\frac{3}{2}$) spin degeneracy. Optical orientation and alignment of excitons can be described by using the spin-density matrix.[3,4,11] In the steady-state regime of photoexcitation the components $\rho_{mm'}$ of the localized-exciton density matrix satisfy the kinetic equation

$$\left(\frac{\partial\rho}{\partial t}\right)_{\text{rec}}+\left(\frac{\partial\rho}{\partial t}\right)_{\text{s.r.}}+\frac{i}{\hbar}[\rho,\mathcal{H}_{\text{exch}}+\mathcal{H}_{\mathbf{B}}]+\hat{G}=0. \tag{1}$$

The terms on the left-hand side take account of the exciton recombination, spin relaxation, exchange, and Zeeman interaction in the presence of magnetic field $\mathbf{B}$, and $\hat{G}$ is the generation matrix. Let $|m\rangle$ be the basis states $|s_z,J_z\rangle$ of the $e1$-hh1$(1s)$ exciton with the angular momentum component $m=s_z+J_z=2,\ 1,\ -1$, and $-2$. In this basis the exchange term in the spin Hamiltonian is given by

$$\mathcal{H}_{\text{exch}}=\frac{\hbar}{2}\begin{bmatrix}-2\omega_0 & 0 & 0 & \omega_1\\ 0 & 0 & \omega_2 & 0\\ 0 & \omega_2 & 0 & 0\\ \omega_1 & 0 & 0 & -2\omega_0\end{bmatrix}, \tag{2}$$

where $\omega_n$ are the exchange interaction constants describing, respectively, the isotropic ($\omega_0$), anisotropic tetragonal ($\omega_1$) and in-plane anisotropic ($\omega_2$) exchange splittings, and the coordinate system with $x\|[110]$, $y\|[\bar{1}10]$ is used. The recombination term has a standard form

$$\left(\frac{\partial\rho_{mm'}}{\partial t}\right)_{\text{rec}}=-\frac{1}{2}\left(\frac{1}{\tau_m}+\frac{1}{\tau_{m'}}\right)\rho_{mm'},\quad \frac{1}{\tau_m}=\frac{1}{\tau_r}\delta_{|m|,1}+\frac{1}{\tau_0}, \tag{3}$$

where $\delta_{m,m'}$ is the Kronecker symbol, $\tau_r$ is the radiative lifetime for the exciton states $|\pm1\rangle$, and $\tau_0^{-1}$ is the nonradiative recombination rate which is usually taken to be the same for all states.

In the following the light polarization is characterized by the degree of circular polarization, $P_c$, and the degrees of linear polarization, $P_l$ and $P_{l'}$, as they refer to the two pairs of rectangular axes $x,y$ and $x'\|[100]$, $y'\|[010]$:

$$P_c=\frac{I_{\sigma_+}-I_{\sigma_-}}{I_{\sigma_+}+I_{\sigma_-}}=\frac{\rho_{1,1}-\rho_{-1,-1}}{\rho_{1,1}+\rho_{-1,-1}},$$

$$P_l=\frac{I_y-I_x}{I_y+I_x}=-\frac{\rho_{1,-1}+\rho_{-1,1}}{\rho_{1,1}+\rho_{-1,-1}},$$

$$P_{l'}=\frac{I_{x'}-I_{y'}}{I_{x'}+I_{y'}}=i\frac{\rho_{1,-1}-\rho_{-1,1}}{\rho_{1,1}+\rho_{-1,-1}}. \tag{4}$$

The PL intensity $I$ given as a sum $I_{\sigma_+}+I_{\sigma_-}$ (or $I_x+I_y$ or $I_{x'}+I_{y'}$, which are equivalent) is proportional to $\rho_{1,1}+\rho_{-1,-1}$.

In order to make transparent the physics of the phenomena under study, here we give a simplified description of the optical orientation and alignment and the orientation-to-alignment conversion induced by a longitudinal magnetic field in type-II SL's. The results of the elaborate theory are presented in Appendix A. For resonant excitation conditions and in the absence of spin relaxation, the optically inactive sublevels remain unpopulated, the only nonzero components of the density matrix $\rho_{mm'}$ are those with $m,m'=\pm1$, and

the $1s$-hh1($1s$) exciton acts as a two-level system. Recall that any two levels can be considered as two states of an effective three-dimensional pseudospin with $S=\frac{1}{2}$. The $2\times 2$ spin density matrix $\rho_{mm'}(m,m'=\pm 1)$ is expressed in terms of the average pseudospin $\mathbf{S}$ as

$$\hat{\rho}=N(\tfrac{1}{2}+\mathbf{S}\sigma), \tag{5}$$

where $\sigma_\alpha$ ($\alpha=x,y,z$) are the Pauli matrices and $N$ is the steady-state exciton concentration. The pure exciton states $|1\rangle$ and $|-1\rangle$ are equivalent to the pseudospin polarized parallel or antiparallel to the $z$ axis, respectively. The exciton states

$$|Y\rangle=-i(|1\rangle-|-1\rangle)/\sqrt{2}, \quad |X\rangle=(|1\rangle+|-1\rangle)/\sqrt{2},$$

dipole-active along the $y\|[110]$ or $x\|[1\overline{1}0]$ axis, are described by a pseudospin with $S_x=\frac{1}{2}$ or $-\frac{1}{2}$, respectively. Finally, the states $|X'\rangle=(|X\rangle+|Y\rangle)/\sqrt{2}$ or $|Y'\rangle=(-|X\rangle+|Y\rangle)/\sqrt{2}$ polarized in the $x'$ and $y'$ directions correspond to a pseudospin with nonzero component $S_y=\frac{1}{2}$ or $-\frac{1}{2}$. Thus one can rewrite Eq. (4) as

$$P_c=2S_z, \quad P_l=-2S_x, \quad P_{l'}=2S_y. \tag{6}$$

The pseudospin Hamiltonian is a sum of the exchange and Zeeman terms,

$$\mathcal{H}=\frac{\hbar}{2}(\omega_2\sigma_x+\Omega_\parallel\sigma_z), \tag{7}$$

where $\hbar\omega_2$ is the zero-field splitting of the radiative doublet introduced in Eq. (2), $\hbar\Omega_\parallel=(g_h^\parallel-g_e^\parallel)\mu_0 B_\parallel$, and $g_e^\parallel$ and $g_h^\parallel$ are the electron and heavy-hole longitudinal $g$ factors. The pseudospin components $S_x^0$, $S_y^0$, and $S_z^0$ describing the initial polarization of photogenerated excitons are related to the Stokes parameters $P_l^0$, $P_{l'}^0$, and $P_c^0$ of the incident light as in Eq. (6). According to Eq. (7) the pseudospin rotates around the vector $\mathbf{\Omega}=(\omega_2,0,\Omega_\parallel)$ with the effective Larmor frequency $\Omega=\sqrt{\Omega_\parallel^2+\omega_2^2}$. If the exciton lifetime $\tau$ is long enough so that $\omega_2\tau\gg 1$ (and this is the case for localized excitons in type-II GaAs/AlAs SL's), then the pseudospin Larmor precession around $\mathbf{\Omega}$ leads to a depolarization of the initial spin component perpendicular to $\mathbf{\Omega}$, while the component parallel to $\mathbf{\Omega}$ remains unchanged. As a result the steady-state pseudospin orientation is obtained by projecting $\mathbf{S}^0$ onto the $\mathbf{\Omega}$ direction

$$\mathbf{S}=\frac{(\mathbf{S}^0\mathbf{\Omega})\mathbf{\Omega}}{\Omega^2}. \tag{8}$$

This simple model naturally explains the interconnection between the orientation and alignment in longitudinal magnetic fields. Let us consider particular cases. If excitons are excited by light polarized along the [110] or [1$\overline{1}$0] axis, then the pseudospin is initially directed parallel or antiparallel to the $x$ axis (Fig. 1). The vector $\mathbf{\Omega}$ lies in the $(x,z)$ plane, and makes an angle $\varphi=\arctan\Omega_\parallel/\omega_2$ with the $x$ axis. According to Eq. (8), the components of the average pseudospin are given by

$$S_x=S_x^0\cos^2\varphi, \quad S_y=0, \quad S_z=S_x^0\cos\varphi\sin\varphi. \tag{9}$$

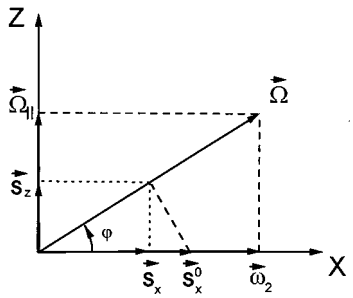


FIG. 1. Schematic representation of the exciton pseudospin projections. $\mathbf{S}_x^0$ is the initial pseudospin vector under [110] linearly polarized excitation; $S_x$ and $S_z$ are the components of the average pseudospin.

Taking into account the relation between $P_l$, $P_c$, and $\mathbf{S}$, we obtain

$$P_l=P_l^0\frac{\omega_2^2}{\omega_2^2+\Omega_\parallel^2}, \quad P_c=-P_l^0\frac{\omega_2\Omega_\parallel}{\omega_2^2+\Omega_\parallel^2}. \tag{10}$$

It follows then that, under linearly polarized excitation along [110] or [1$\overline{1}$0], the longitudinal magnetic field gives rise to two effects: (a) suppression of the alignment and (b) polarization conversion with the appearance of circular polarization in the PL. For circularly polarized excitation the initial pseudospin $\mathbf{S}^0$ is directed along $z$. At zero magnetic field the vectors $\mathbf{S}^0$ and $\mathbf{\Omega}$ are perpendicular and, for $\omega_2\tau\gg 1$, the exciton PL is unpolarized. The longitudinal magnetic field restores the PL circular polarization and induces the linear polarization $P_l$. According to Eq. (8), both effects are described by

$$P_c=P_c^0\frac{\Omega_\parallel^2}{\omega_2^2+\Omega_\parallel^2}, \quad P_l=-P_c^0\frac{\omega_2\Omega_\parallel}{\omega_2^2+\Omega_\parallel^2}. \tag{11}$$

Under excitation by light polarized in the $x'$ (or $y'$) direction, the vector $\mathbf{S}^0$ is orthogonal to the $(x,z)$ plane, and the spin precession suppresses the PL polarization. Since in type-II GaAs/AlAs SL's there are two kinds of localized excitons with $\omega_2$ differing in sign, the conversion terms in Eqs. (10) and (11) have to be multiplied by the interface preference factor $f$.

With allowance for the spin relaxation, one has to include the inactive states $|\pm 2\rangle$ into consideration, and analyze a four-level system. The general equations for the PL polarization in the presence of a magnetic field are derived in Appendix A. With the help of relations (A5) between exciton parameters in type-II GaAs/AlAs SL's, one finds that

$$P_c=b\frac{\Omega_\parallel^2 P_c^0-f\omega_2\Omega_\parallel P_l^0}{a\Omega_\parallel^2+\omega_2^2},$$

$$P_l=b\frac{-f\omega_2\Omega_\parallel P_c^0+\omega_2^2 P_l^0}{a\Omega_\parallel^2+\omega_2^2}, \quad P_{l'}=0, \tag{12}$$

where

$$a=\eta\left(1-\frac{\tilde{T}_1\tilde{T}_{0,1}}{(\tau_{s,1}^-)^2}\right), \quad b=\eta N, \tag{13}$$

and other notations are introduced in Appendix A. One can see that Eq. (12) differs from Eqs. (10) and (11) by a common factor $b$ and the coefficient $a$ in the denominators. It is worth mentioning that equations similar to Eq. (12) are derived from the two-level model by introducing an anisotropic effective-pseudospin lifetime $\tau_{s,\parallel}$ for $S_z$, and $\tau_{s,\perp}$ for $S_x, S_y$. In this case the parameters $a$ and $b$ are given, respectively, by $T_\perp/T_\parallel$ and $T_\perp/\tau$, where the effective lifetimes of optical orientation and alignment are defined as $T_\parallel^{-1}=\tau^{-1}+\tau_{s,\parallel}^{-1}$ and $T_\perp^{-1}=\tau^{-1}+\tau_{s,\perp}^{-1}$.

As mentioned above, in type-II GaAs/AlAs SL's, the exchange splitting $\omega_2$ exceeds the inverse characteristic lifetime of localized excitons. It should be noted that at fields up to 3 T the exciton radius changes only a few percent, so that one does not expect the localization dynamics to change significantly with magnetic field. However the value of $\omega_2$ is small enough to be comparable with the inverse lifetime, $\tau_f^{-1}$, of free excitons. This means that, in general, the generation rates to sublevels of the localized exciton are field dependent. Recall that the radiative doublet of the free-exciton state in type-II SL's is degenerate.[14] The longitudinal magnetic field splits the doublet into the $|\pm 1\rangle$ states. This splitting rotates and depolarizes the aligned exciton oscillating dipole moments, while having no effect on the exciton spin orientation.[1] Analytically, the field dependence of the effective feeding rates is taken into account if the polarization $P_l^0$ in Eq. (12) is replaced by

$$P_l^0(B_\parallel)=\frac{\mathcal{P}_l^0+\Omega_\parallel\tau_f\mathcal{P}_{l'}^0}{1+\Omega_\parallel^2\tau_f^2}, \tag{14}$$

while $P_c^0$ is kept field independent. Here $\mathcal{P}_l^0$ and $\mathcal{P}_{l'}^0$ are defined via the generation matrix $G_{mm'}$ as free-exciton states similar to Eq. (4), and we neglect the spin relaxation of free excitons during their lifetime $\tau_f$, governed mostly by the free-exciton localization processes.

## III. EXPERIMENTAL TECHNIQUES AND SAMPLE PREPARATION

The results presented below were obtained on two samples labeled NMSL-3 and NMSL-7. The samples are type-II GaAs/AlAs SL's grown by molecular beam epitaxy on a fixed semi-insulating GaAs substrate at roughly 600 °C in a RIBER-32 installation. The thicknesses of the GaAs and AlAs layers are practically the same within the sample area ($3\times 3\ \mathrm{mm}^2$ for NMSL-3 and $3\times 6\ \mathrm{mm}^2$ for NMSL-7). The NMSL-3 SL consists of 80 periods, each made up of seven GaAs and four AlAs monomolecular layers (mls). In the case of NMSL-7, there are seven periods; each period consists of 7.2-ml GaAs, 5.7-ml AlAs, 8-ml GaAs, and 5.7-ml AlAs. In both samples there were 60- and 10-s growth interruptions under As flux after each GaAs and AlAs layer, respectively. In the case of NMSL-7 only, there are 0.5-$\mu$m $Al_{0.43}Ga_{0.57}As$ layers above and below the SL stack.

The samples were mounted in a liquid-helium cryostat ($T=4.2$ K), and photoexcited by a $Kr^+$ laser ($\lambda=6471$ Å) beam of intensity $\sim 6\ \mathrm{mW\ cm^{-2}}$. It is worth noting that an increase in the pumping intensity leads to a rapid suppression of the alignment, whereas, in the same intensity range, the optical orientation almost retains its value. This can be explained in terms of photoinduced enhancement of the spin relaxation for one of two particles, an electron or a hole, bound into an exciton. The PL was measured in the backscattering geometry at a small angle to the excitation axis. Just as in Ref. 11, the low-temperature PL line is due to the radiative recombination of excitons formed by $X_z$-valley electrons confined predominantly in AlAs layers, and heavy holes confined predominantly in GaAs layers.

In the following we use the abbreviation $I_\beta^\alpha$ to designate the intensity of secondary emission (luminescence) in the configuration $(\alpha,\beta)$ of the polarizer and analyzer, where $\alpha$ and $\beta$ are linear polarizations along the axes [100], [010], [110], and [1$\bar{1}$0], or circular polarizations $\sigma_+$ and $\sigma_-$. Instead of measuring the polarization degrees $P_c^\alpha=(I_{\sigma_+}^\alpha-I_{\sigma_-}^\alpha)/(I_{\sigma_+}^\alpha+I_{\sigma_-}^\alpha)$, $P_l^\alpha$ and $P_{l'}^\alpha$ defined in accordance with Eq. (4), we applied the modulation technique where the analyzer is in a fixed position and the sample is pumped by the incident light changing its polarization from circular or linear to orthogonal at a frequency of 26.61 kHz. The measured values are then the effective polarization degrees

$$\rho_\alpha^c=\frac{I_\alpha^{\sigma_+}-I_\alpha^{\sigma_-}}{I_\alpha^{\sigma_+}+I_\alpha^{\sigma_-}},\quad \rho_\alpha^l=\frac{I_\alpha^{110}-I_\alpha^{1\bar{1}0}}{I_\alpha^{110}+I_\alpha^{1\bar{1}0}},\quad \rho_\alpha^{l'}=\frac{I_\alpha^{100}-I_\alpha^{010}}{I_\alpha^{100}+I_\alpha^{010}}. \tag{15}$$

This technique of modulating the incident-light polarization minimizes anticrossing effects. The equivalence between this set and the values of $P_c^\alpha$, $P_l^\alpha$ and $P_{l'}^\alpha$ is demonstrated in Appendix B. The incident-light polarization was modulated by a photoelastic modulator.[16] To detect the linear polarization, a linear polarizer was installed in the luminescence detection channel with a proper choice of the rotation angle. For measurements of circularly polarized components, we used a circular-polarization analyzer consisting of a quarter-wavelength plate and a linear polarizer with the transmission axis of the latter, making an angle of 45° with the plate principal axis.

## IV. OPTICAL ORIENTATION AND ALIGNMENT OF EXCITONS: EXPERIMENTAL RESULTS AND DISCUSSION

The PL spectra of the samples NMSL-3 and NMSL-7 consist of a main line due to the no-phonon recombination of type-II localized excitons and of phonon replicas.[17] Figure 2 displays the dependences $\rho_\alpha^c(B_\parallel)$ and $\rho_\alpha^l(B_\parallel)$ measured on the sample NMSL-7 at the PL spectral maximum ($\lambda=6684$ Å). The polarization properties of the phonon replicas are similar to those of the no-phonon line. It is seen from Fig. 2(a) that $\rho_{\sigma_+}^c(B_\parallel)$ rapidly increases and saturates from 2.5% to 5% in weak magnetic fields $B_\parallel\approx 20$ G, and then gradually increases up to the level of 20% at $B_\parallel=2.5$ kG. Figure 2(b) clearly demonstrates the field-induced orientation-to-alignment conversion: $\rho_{110}^c(B_\parallel)$ reaches a maximum value of 5% at $B_\parallel\approx 0.7$ kG, and reverses its sign under the field inversion. Moreover, $\rho_{110}^c(B_\parallel)$ differs in sign from the measured dependence $\rho_{1\bar{1}0}^c(B_\parallel)$. The effect of longitudinal magnetic field upon the optical alignment is illustrated in Fig. 2(c). Note that the main variation of $\rho_{110}^l$ takes

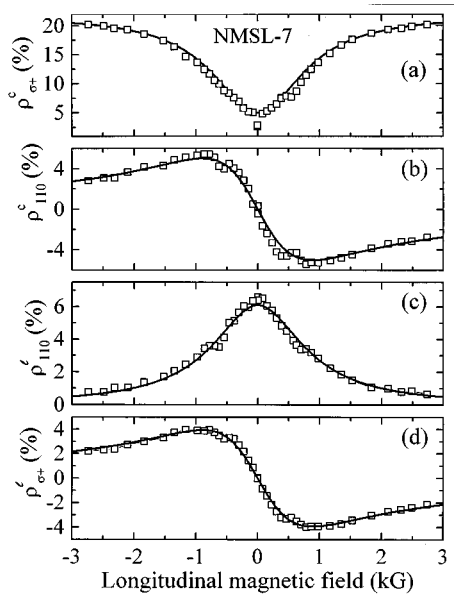


FIG. 2. Effect of the longitudinal magnetic field on optical orientation and alignment of localized excitons in the sample NMSL-7: (a) $\rho^c_{\sigma_+}$, (b) $\rho^c_{110}$, (c) $\rho^l_{110}$, and (d) $\rho^l_{\sigma_+}$. Experimental data ($T=4.2$ K) are shown as points. Solid curves are theoretical fits to Eq. (10). The anticrossing features superimposed on the experimental dependences are small, and were not taken into account in the calculations.

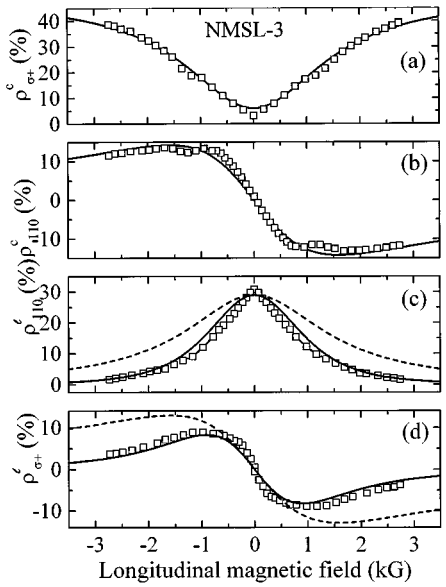


FIG. 3. The effective polarization degrees $\rho^c_{\sigma_+}$ (a), $\rho^c_{110}$ (b), $\rho^l_{110}$ (c), and $\rho^l_{\sigma_+}$ (d) as functions of the longitudinal magnetic field for the sample NMSL-3. Note the nonequivalence between the orientation-to-alignment and alignment-to-orientation conversions. Dashed curves are calculated by using Eq. (10) and neglecting the cascade character of localized-exciton formation; solid curves are theoretical fits to Eq. (10), which accounts for cascading with $P^0_l$ given by Eq. (14).

place at the same magnetic fields $B_\parallel \approx 0.7$ kG as for the function $\rho^c_{\sigma_+}(B_\parallel)$ in Fig. 2(a). Comparison of Figs. 2(d) and 2(b) shows that, for the sample NMSL-7, the orientation-to-alignment effect is reversible: the experimental dependences $\rho^c_{110}(B_\parallel)$ and $\rho^l_{\sigma_+}(B_\parallel)$ are close to each other.

We attribute the fast low-field increase of $\rho^c_{\sigma_+}$ in Fig. 2(a) to spatially separated electron-hole pairs characterized by small values of exchange splittings.[18] In the following analysis this contribution is taken into account by adding a constant value of 5% to the theoretical curve $\rho^c_{\sigma_+}(B_\parallel)$. Except for this narrow region the four dependences of Fig. 2 can be described by using Eq. (12) and neglecting the influence of the field on the exciton polarization at the intermediate stage before the exciton is trapped into a localized state. If excitons are generated resonantly (which is virtually impossible if there is inhomogeneous broadening), $bP^0_c$ and $bP^0_l$ in Eq. (12) would be given by theory. Since the photoexcitation here is only quasiresonant (i.e., at slightly higher energy), they are treated as fitting parameters since excitons can be formed both by direct excitation and by binding of an electron and hole with uncorrelated spins, i.e., excited by two separated photon absorption events. One can deduce the following relations from Eq. (12):

$$\frac{\rho^c_{\sigma_+}}{\rho^c_{110}} = -\frac{1}{f}\frac{\Omega_\parallel}{\omega_2}, \quad \frac{\rho^l_{\sigma_+}}{\rho^l_{110}} = -f\frac{\Omega_\parallel}{\omega_2}, \quad \frac{\max|\rho^l_{\sigma_+}|}{\rho^l_{110}(0)} = \frac{|f|}{2\sqrt{a}}, \tag{16}$$

which can be used to evaluate unambigously $\omega_2/(g^\parallel_h - g^\parallel_e)$, $\sqrt{a}$ and $f$. The curves in Fig. 2 are calculated for $bP^0_c = 7.6\%$, $bP^0_l = 6.1\%$, $\hbar\omega_2 = 1.8$ $\mu$eV, $a = 0.45$, and $f = 0.9$. In order to find $\omega_2$ we extrapolated $g^\parallel_e = 1.91$ and $g^\parallel_h = 2.43$ for NMSL-7 from Ref. 19. One can see that the anticrossing features superimposed on the experimental dependences in Fig. 2 are indeed small, and do not prevent the evaluation of $\omega_2$, $\sqrt{a}$, and $f$. The least-squares analysis shows that these parameters are determined within accuracy of 3% for $f$, 12 % for $\sqrt{a}$, and 8% for $\omega_2$.

The magnetic-field dependences of $\rho^c_{\sigma_+}$, $\rho^c_{110}$, $\rho^l_{110}$, and $\rho^l_{\sigma_+}$ for the sample NMSL-3 are shown in Fig. 3. The main field-induced effects, namely, the restoration of optical orientation, suppression of optical alignment and polarization conversion, are also observed in NMSL-3. However, as compared to Fig. 2, one should note two remarkable differences. First, the effective polarization degrees $\rho^c_{110}$ and $\rho^l_{\sigma_+}$ reach their maxima at different values of $B_\parallel$, 1 and 0.7 kG, respectively. In other words, the orientation-to-alignment and alignment-to-orientation conversions are nonequivalent. Second, the characteristic magnetic fields governing the increasing orientation ($\rho^c_{\sigma_+}$) and decreasing alignment ($\rho^l_{110}$) also differ by a factor of $\sim 1.5$. As shown in Appendix B, this result can be related to a two-step or multistep process of localized-exciton formation. We explain the different shapes of the curves $\rho^c_{110}(B_\parallel)$ and $\rho^l_{\sigma_+}(B_\parallel)$ in Fig. 3 by the Hanle effect on the free-exciton alignment described by Eq. (14).

To further test the cascade model, we performed measurements of the linear polarization in the axes [110] and [1$\bar{1}$0] under linear [100]-to-[010] modulated excitation (Fig. 4). According to Eqs. (12) and (14) this kind of polarization conversion is described by

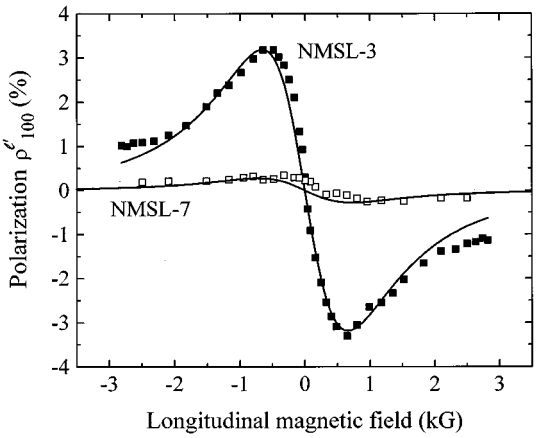


FIG. 4. The effective polarization degree $\rho_{110}^{l'}$ as a function of the longitudinal magnetic field for the samples NMSL-7 (open squares) and NMSL-3 (full squares). The [100]-to-[110] conversion occurs due to the Hanle effect at intermediate stage of the cascade localized-exciton formation. The solid curves *a* and *b* are the best fit to Eq. (17) obtained for $\tau_f = 190$ and 230 ps, respectively.

$$\rho_{110}^{l'}(B_\parallel) = b\mathcal{P}_{l'}^0 \frac{\omega_2^2}{a\Omega_\parallel^2 + \omega_2^2} \frac{\Omega_\parallel \tau_f}{1+\Omega_\parallel^2 \tau_f^2}, \tag{17}$$

and, for comparable $\omega_2$ and $\tau_f^{-1}$, exceeds by far the $P_{l'}^0 \to P_l$ conversion obtained in the one-step model, see Eq. (A2). One can conclude that, for the sample NMSL-7, the [100]-to-[110] conversion is ineffective, whereas in the sample NMSL-3 the longitudinal magnetic field induces a rather strong transformation from the [100] to [110] linear polarization. The set of parameters for the sample NMSL-3 used to calculate the solid curves in Fig. 3 from Eqs. (12) and (14) is as follows: $g_e^\parallel = 1.91$ and $g_h^\parallel = 2.6$,[19] $bP_c^0 = 32\%$, $b\mathcal{P}_l^0 = 29\%$, $\hbar\omega_2 = 5\ \mu$eV, $a = 0.74$, $f = 0.77$, and $\tau_f = 110$ ps. Just as for the sample NMSL-7, the anticrossing features play a minor role. The NMSL-3 curve in Fig. 4 is calculated for the same values of $a$ and $\omega_2$ as in Fig. 3, and for $b\mathcal{P}_{l'}^0 = 5.5\%$ and $\tau_f = 230$ ps. The difference by a factor of $\sim 2$ between the values of $\tau_f$ obtained from Figs. 3 and 4 can be explained as follows. Under quasiresonant excitation, localized excitons are partially generated from low-energy free excitons with comparatively long lifetimes, and they are partially created from hot excitons or electron-hole pairs characterized by short lifetimes. The polarization conversion shown in Fig. 4 is completely due to the cascade via long-lived free excitons, whereas the polarization signal in Fig. 3 has contributions from all localized excitons irrespective of their generation mechanism. The true value of the free-exciton lifetime follows from fitting the data of Fig. 4, and the effective time deduced from Fig. 3 can be shorter. The observation of the signal $\rho_{110}^{l'}(B_\parallel)$ is a direct evidence of the exciton cascade kinetics. The NMSL-7 curve in Fig. 4 is calculated for $\tau_f = 190$ ps, which is of the same order of magnitude as for the sample NMSL-3.

The absolute values of characteristic lifetimes can also be determined. According to Eq. (A2) the zero-field value of $P_{l'}$ excited by the light linearly polarized along [100] or [010] is of the order of $(\omega_2 T_i)^{-2}$. In order to determine $T_i$ in absolute units, it is more convenient to measure the zero-field polarization $P_{l'}$ under circularly polarized excitation. In fact, from Eq. (A6) the zero-field value of $|\rho_{100}^c|$ is given by

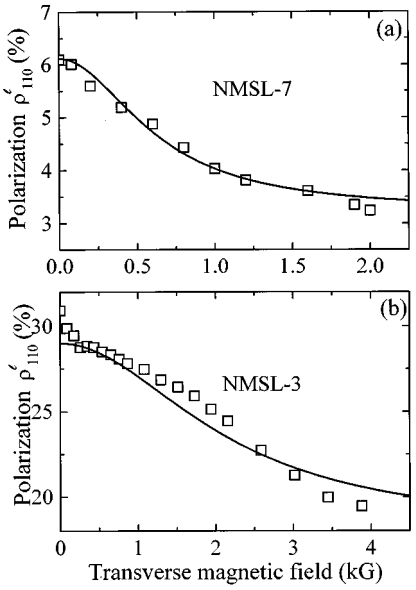


FIG. 5. Effect of the transverse magnetic field on the exciton alignment in the samples NMSL-7 (a) and NMSL-3 (b). The solid curves are calculated in the one-step model for $\hbar\omega_0 = 5.8\ \mu$ eV (a) and 19 $\mu$ eV (b).

$$|\rho_{100}^c(0)| = |P_c^0| \frac{bf}{\omega_2 T_2}, \tag{18}$$

and is proportional to the first power of $(\omega_2 T_2)^{-1}$. We measure for the sample NMSL-3 $|\rho_{100}^c(0)| \approx 2.8\%$ and for the sample NMSL-7 $|\rho_{100}^c(0)| = (0.8 \pm 0.05)\%$, which gives $T_2 = 1.1$ ns and $T_2 = 3.0$ ns, respectively, where $T_2$ is defined by Eq. (A4).

The other characteristic times can be determined by transverse magnetic-field measurements. Figure 5 displays the variation of $\rho_{110}^l$ in a transverse magnetic field measured on the samples NMSL-7 (a) and NMSL-3 (b), respectively. In both cases the value of $\rho_{110}^l$ eventually decreases by a factor of $\sim 2$. In agreement with the theory, the shape of the curve $\rho_{110}^l$ is insensitive to the vector direction of $\mathbf{B}_\perp$ in the interface plane.

In contrast to $\rho_{110}^l$, the PL intensity exhibits no remarkable change in the magnetic-field range studied. According to Eq. (A9) the near equality of $I(0)$ and $I(B_\perp \to \infty)$ can be naturally explained by an inefficient nonradiative channel, i.e., by assuming $\tau_0 \gg \tau, \tau_{s,i}$. In this case one has, instead of Eq. (A9),

$$\frac{P_l(0)}{P_l(\infty)} - 1 \approx \frac{1}{1+(\tau_{s,2}^+/2\tau)},$$

$$h'^2 = \frac{1}{2}\frac{\tau_{s,2}^+}{\tau_{s,2}^h}\left(1+\frac{\tau_{s,2}^h}{2\tau}\right)\frac{1+(\tau_{s,2}^+/4\tau)}{1+(\tau_{s,2}^+/2\tau)}\left(\frac{\Omega_\perp}{\omega_0}\right)^2. \tag{19}$$

From Fig. 5(a) and the above equation, one can obtain $\tau_{s,2}^+/\tau = 0.21$. In order to estimate the ratio of the electron and hole spin-relaxation times further, we will ignore their possible anisotropy and assume $\tau_{s1}^e = \tau_{s2}^e \equiv \tau_s^e$ and $\tau_{s1}^h = \tau_{s2}^h \equiv \tau_s^h$.

Then, from parameter $a$, we find $|\tau_s^-|/\tau_s^+ = 2.3$ for the sample NMSL-7, and, under a reasonable assumption $\tau_s^e > \tau_s^h$, come to $\tau_s^h/\tau_s^e = 0.4$. The solid curve in Fig. 5(a) is calculated by using Eqs. (A8) and (19) for $g_e^\perp \approx g_e^\parallel$,[19] and $\hbar\omega_0 = 5.8\ \mu$eV as a fitting parameter. This value of exchange splitting between $|\pm 1\rangle$ and $|\pm 2\rangle$ is in agreement with the theory[14] as well as with the position of level-anticrossing features on the $\rho_\alpha(B_\parallel)$ dependences. Now we can use the measured value of $T_2$ to determine other characteristic times for NMSL-7 in absolute units: $\tau = 32$ ns, $\tau_s^e = 12$ ns, and $\tau_s^h = 4.7$ ns. From Fig. 5(b) we find, for the sample NMSL-3, $\tau_s^+/\tau = 1.85$, $\tau = 2.3$ ns, and $\tau_s^e \approx \tau_s^h = 4.2$ ns. The value of $\hbar\omega_0 = 19\ \mu$eV deduced from the shape of $\rho_{110}^l(B_\perp)$ differs from the theoretical prediction $\hbar\omega_0 = 15\ \mu$eV,[14] and from the result of level-anticrossing analysis, $\hbar\omega_0 = 14\ \mu$eV. This difference may be related to the anisotropy of spin-relaxation times as well as to the cascade character of photoexcitation neglected while calculating the solid curve in Fig. 5(b). Note that the lifetime 2.3 ns for the 20-Å/11-Å sample NMSL-3 is remarkably shorter than that measured for the 22-Å/11.5-Å GaAs/AlAs SL by time-resolved spectroscopy.[8] Since the layer thicknesses in the structure NMSL-3 lie on the border between the type-II and I regions,[17] the exciton lifetime should be very sensitive to the sample growth conditions. Therefore time-resolved measurements on the samples under study are of special interest.

## V. SUMMARY

Polarized steady-state PL spectroscopy has been used to study exciton optical orientation and alignment in type-II GaAs/AlAs superlattices. The spin-density matrix formalism in the one- and two-step models has been developed to relate the Stokes polarization parameters of the incident and secondary radiation including the linear-to-circular polarization conversion. Experimentally, six of the total nine polarization relations, namely, $P_c$-$P_c^0$, $P_l$-$P_l^0$, $P_c$-$P_l^0$, $P_l$-$P_c^0$, $P_{l'}$-$P_c^0$, and $P_l$-$P_{l'}^0$, have been measured as a function of the longitudinal magnetic field. The transverse magnetic-field effect on the PL intensity and the linear polarization $P_l$ has provided a complementary insight into the excitonic kinetics. Comparison between the theory and the experimental data obtained in both the longitudinal and transverse magnetic fields has made it possible to determine the fine structure and kinetic parameters of the localized-exciton ground-state quartet in the regime of low-intensity excitation where effects of exciton-exciton and free carrier-exciton interactions are excluded. The linear [100]-to-[110] conversion induced by the longitudinal magnetic field is a signature of the exciton cascade kinetics. The field-induced linear-to-circular polarization conversion provides an effective method to measure the interface preference factor $f$, which is expected to be an important diagnostic tool in studying quantum-well interfaces.

## ACKNOWLEDGMENTS

Support from NSF Divisions of Materials Research and International Programs is gratefully acknowledged.

## APPENDIX A

We assume the mechanisms of electron and hole spin relaxation in the exciton to be independent, and the exchange splitting to be small compared with the thermal energy, in which case the spin relaxation term in the kinetic equation (1) has the form

$$\left(\frac{\partial\rho_{sj,s'j'}}{\partial t}\right)_{s.r.} = -\delta_{ss'}\frac{1}{\tau_{s,1}^e}\left(\rho_{sj,sj'} - \frac{1}{2}\sum_{s''}\rho_{s''j,s''j'}\right) - \delta_{jj'}\frac{1}{\tau_{s,1}^h}\left(\rho_{sj,s'j} - \frac{1}{2}\sum_{j''}\rho_{sj'',s'j''}\right) - \left[(1-\delta_{ss'})\frac{1}{\tau_{s,2}^e} + (1-\delta_{jj'})\frac{1}{\tau_{s,2}^h}\right]\rho_{sj,s'j'}, \tag{A1}$$

where the times $\tau_{s,1}^e$ and $\tau_{s,2}^e$ (or $\tau_{s,1}^h$ and $\tau_{s,2}^h$) describe the relaxation of spin-density matrix components $\rho_{sj,s'j'}$ diagonal and off-diagonal with respect to the electronic indices $s,s'$ (or the hole indices $j,j'$).

*Longitudinal magnetic field.* From the explicit solution of Eq. (1) in a longitudinal magnetic field $\mathbf{B}\|z$, we obtain the following relations between the PL and incident-light polarizations:

$$P_c = N\frac{(1+\Omega_\parallel^2T_2^2)(P_c^0+Q\widetilde{P}_c^0) - f\omega_2\Omega_\parallel T_2^2P_l^0 + f\omega_2T_2P_{l'}^0}{(1+\Omega_\parallel^2T_2^2)(1-S)+\omega_2^2T_2\widetilde{T}_1},$$

$$P_l = N\frac{-f\omega_2\Omega_\parallel T_2^2(P_c^0+Q\widetilde{P}_c^0) + (1+\omega_2^2T_2\widetilde{T}_1-S)\,\eta P_l^0 + \Omega_\parallel T_2(1-S)\,\eta P_{l'}^0}{(1+\Omega_\parallel^2T_2^2)(1-S)+\omega_2^2T_2\widetilde{T}_1}, \tag{A2}$$

$$P_{l'} = N\frac{-f\omega_2T_2(P_c^0+Q\widetilde{P}_c^0) - \Omega_\parallel T_2(1-S)\,\eta P_l^0 + (1-S)\,\eta P_{l'}^0}{(1+\Omega_\parallel^2T_2^2)(1-S)+\omega_2^2T_2\widetilde{T}_1},$$

where $\widetilde{P}_c^0=(G_{2,2}-G_{-2,-2})/(G_{1,1}+G_{-1,-1})$, and $P_c^0$, $P_l^0$, and $P_{l'}^0$, are defined via the generation matrix components $G_{mm'}$, just as $P_c$, $P_l$, and $P_{l'}$ are related to $\rho_{mm'}$ in Eq. (4). The interface preference factor $f$ is the difference between the fractions of excitons with positive and negative values of $\omega_2$. Other notations are as follows:

$$Q=\frac{\widetilde{T}_{0,1}}{\tau_{s,1}^-}\frac{1+(\Omega_\parallel' T_{0,2})^2}{1+(\Omega_\parallel' T_{0,2})^2+\omega_1^2 T_{0,2}\widetilde{T}_{0,1}},$$

$$S=\frac{\widetilde{T}_1}{\tau_{s,1}^-}Q=\frac{\widetilde{T}_1\widetilde{T}_{0,1}}{(\tau_{s,1}^-)^2}\frac{1+(\Omega_\parallel' T_{0,2})^2}{1+(\Omega_\parallel' T_{0,2})^2+\omega_1^2 T_{0,2}\widetilde{T}_{0,1}}, \quad \text{(A3)}$$

$$\eta=\frac{T_2}{\widetilde{T}_1}, \quad N=\frac{1-\widetilde{T}_1\widetilde{T}_{0,1}(\tau_{s,1}^+)^{-2}}{1+\widetilde{T}_{0,1}(\tau_{s,1}^+)^{-1}p}, \quad p=\frac{G_{2,2}+G_{-2,-2}}{G_{1,1}+G_{-1,-1}},$$

$$\frac{1}{T_i}=\frac{1}{\tau}+\frac{2}{\tau_{s,i}^+}, \quad \frac{1}{\widetilde{T}_i}=\frac{1}{\tau}+\frac{1}{\tau_{s,i}^+},$$

$$\frac{1}{T_{0,i}}=\frac{1}{\tau_0}+\frac{2}{\tau_{s,i}^+}, \quad \frac{1}{\widetilde{T}_{0,i}}=\frac{1}{\tau_0}+\frac{1}{\tau_{s,i}^+}, \quad \text{(A4)}$$

$$\frac{1}{\tau}=\frac{1}{\tau_r}+\frac{1}{\tau_0}, \quad \frac{1}{\tau_{s,i}^\pm}=\frac{1}{2}\left(\frac{1}{\tau_{s,i}^e}\pm\frac{1}{\tau_{s,i}^h}\right) \quad (i=1,2).$$

$\tau$ is the lifetime of the dipole-active states $|\pm 1\rangle$ including both radiative and nonradiative decay; $\hbar\Omega_\parallel=(g_h^\parallel-g_e^\parallel)\mu_0 B_\parallel$ and $\hbar\Omega_\parallel'=(g_h^\parallel+g_e^\parallel)\mu_0 B_\parallel$ are the Zeeman splittings between the states $|1\rangle$ and $|-1\rangle$ and between the states $|2\rangle$ and $|-2\rangle$, respectively; $g_e^\parallel$ and $g_h^\parallel$ are the longitudinal components of the electron and hole $g$ factors; and $\mu_0$ is the Bohr magneton. While deriving Eq. (A2), we assumed $G_{mm'}=0$ for the pairs $m=\pm 1$, $m'=\pm 2$ or $m=\pm 2$, $m'=\pm 1$ or $m=-m'=\pm 2$. Note that, under resonant excitation, excitons are generated directly into the states $|\pm 1\rangle$, so $G_{m,m'}\neq 0$ only for $m,m'=\pm 1$. Under off-resonant excitation, an exciton can be formed by binding of an electron and a hole which may not have been generated by the same photon; i.e., their spins are uncorrelated, so that all of the diagonal components of $\hat{G}$ may be nonzero.

Now we take into account that, in type-II GaAs/AlAs SL's,

$$1\ll\omega_2 T_i, \quad |\omega_1|<\omega_2, \quad g_h^\parallel-g_e^\parallel\ll g_h^\parallel+g_e^\parallel. \quad \text{(A5)}$$

Neglecting terms of the first and higher orders in $(\omega_2 T_i)^{-1}\ll 1$, and assuming the generation to occur only into the optically active states, i.e., $G_{m,m'}=0$ for $m$ or $m'=\pm 2$, we can transform Eq. (A2) into Eq. (12). The polarization $P_{l'}$ appears only in the first order in $(\omega_2 T_i)^{-1}$:

$$P_{l'}=-\frac{b}{T_2}\frac{f\omega_2 P_c^0+a\Omega_\parallel P_l^0}{a\Omega_\parallel^2+\omega_2^2}. \quad \text{(A6)}$$

In the model under consideration the total intensity $I$ is independent of both the incident polarization and the longitudinal magnetic-field. It should be mentioned, however, that in two narrow regions of magnetic field values, the polarization and intensity may behave in a nonmonotonic resonant way.[20,18] These are the so-called anticrossing points where one of the inactive sublevels $|\pm 2\rangle$ crosses the sublevels of the radiative doublet. The theory of localized-exciton level anticrossing was developed by Ivchenko and Kaminski.[21] The anticrossing signals are superimposed on the smooth magnetic-field dependences given by Eq. (A2); their detailed comparison with experiment lies beyond the scope of the present paper. We also neglect the thermal polarization arising due to the temperature dependent difference between the probability rates for intersublevel transitions $E_i\to E_j$ and $E_j\to E_i$, where the indices $i,j$ enumerate the eigenvalues of the Hamiltonian $\mathcal{H}_{\rm exch}+\mathcal{H}_{\mathbf{B}}$. The criterion for validity of this approximation is $|E_i-E_j|\ll k_B T$ ($k_B$ is the Boltzmann constant, and $T$ is the temperature).

*Transverse magnetic field.* In a transverse field $\mathbf{B}\perp z$, the total radiation intensity $I$ and the linear polarization $P_l$ are given by

$$I(B_\perp)=I(\infty)+\frac{I(0)-I(\infty)}{1+h^2}, \quad \text{(A7)}$$

$$P_l I=(P_l I)_\infty+\frac{(P_l I)_0-(P_l I)_\infty}{1+h'^2}, \quad \text{(A8)}$$

where

$$I(\infty)\propto\frac{\tau\tau_0}{\tau+\tau_0}(1+p), \quad \frac{I(0)}{I(\infty)}=1+\frac{\tau_{s,1}^+}{\tau+\tau_0+\tau_{s,1}^+}\frac{(\tau/\tau_0)-p}{1+p},$$

$$\frac{(P_l I)_0}{(P_l I)_\infty}-1=\frac{1+(\tau_{s,2}^+/2\tau_0)}{1+(\tau_{s,2}^+/2\tau)},$$

$$h^2=\frac{T_e\tau_{s,1}^+(\tau+\tau_0)}{\tau+\tau_0+\tau_{s,1}^+}\Omega_\perp^2, \quad h'^2=(T_2+T_{0,2})T_h\Omega_\perp^2, \quad \text{(A9)}$$

$$T_e=\frac{1}{2\omega_0^2}\left(\frac{1}{\tau}+\frac{1}{\tau_{s,2}^e}\right), \quad T_h=\frac{1}{2\omega_0^2}\left(\frac{1}{\tau}+\frac{1}{\tau_{s,2}^h}\right). \quad \text{(A10)}$$

$\hbar\Omega_\perp=g_e^\perp\mu_0 B_\perp$, $g_e^\perp$ is the transverse component of the electron $g$ factor, and it is taken into account that for the heavy holes the transverse $g$ factor is zero. Equations (A7) and (A8) are derived neglecting terms of the order $(\omega_0 T)^{-1}$ and $(\omega_2 T)^{-1}\ll 1$. In this approximation $P_c$ and $P_{l'}=0$, and $I$ and $P_l$ are independent of the orientation of the transverse magnetic field in the $(x,y)$ plane.

## APPENDIX B

The equivalence between the PL polarization degrees $P_c$, $P_l$, and $P_{l'}$ and the measured degrees $\rho_\alpha^c$, $\rho_\alpha^l$, and $\rho_\alpha^{l'}$ [see Eq. (15)] is a consequence of the linear relation

$$P_\gamma=\Lambda_{\gamma\gamma'}P_{\gamma'}^0(\gamma,\gamma'=c,l,l') \quad \text{(B1)}$$

between the PL and incident-light polarizations [see Eq. (A2)] which is true as long as the thermal polarization and level-anticrossing effects are neglected. For example, that $P_c^{110}$ and $\rho_{110}^c$ are the same is demonstrated by using the equation

$$I^{110}_{\sigma_\pm}=I^{1\bar{1}0}_{\sigma_\mp}=I\frac{1\pm\Lambda_{\rm cl}}{2}, \tag{B2}$$

that follows from Eq. (B1).

In the one-step model used to derive Eqs. (A2) or (12), the identity of the functions $P_l^{\sigma_+}(B_\parallel)$ and $P_c^{110}(B_\parallel)$ or of the functions $\rho^c_{110}(B_\parallel)$ and $\rho^l_{\sigma_+}(B_\parallel)$ is a consequence of the time inversion and space symmetries, as well as a result of exclusion of the thermal polarization and level anticrossing effects from consideration. Recall that

$$\rho^c_{110}=\frac{I^{\sigma_+}_{110}-I^{\sigma_-}_{110}}{I^{\sigma_+}_{110}+I^{\sigma_-}_{110}},\quad \rho^l_{\sigma_+}=\frac{I^{110}_{\sigma_+}-I^{1\bar{1}0}_{\sigma_+}}{I^{110}_{\sigma_+}+I^{1\bar{1}0}_{\sigma_+}}.$$

Time-inversion symmetry imposes the following relations on the PL intensities $I^\alpha_\beta$ measured in the backscattering geometry at normal incidence:

$$I^\alpha_\beta(B_\parallel)=I^{\bar{\beta}}_{\bar{\alpha}}(-B_\parallel). \tag{B3}$$

Here, for the linear polarization, $\bar{\alpha}=\alpha$ and, for the circular polarization, $\bar{\alpha}=\sigma_\mp$ if $\alpha=\sigma_\pm$. The GaAs/AlAs single-interface point symmetry $C_{2v}$ imposes the relation

$$I^\alpha_\beta(B_\parallel)=I^{\tilde{\alpha}}_{\tilde{\beta}}(-B_\parallel), \tag{B4}$$

where $\tilde{\alpha}=\alpha$ for the linear polarization along [110] or [$1\bar{1}0$], $\tilde{\alpha}=[010]$ if $\alpha=[100]$, $\tilde{\alpha}=[100]$ if $\alpha=[010]$, and $\tilde{\alpha}=\sigma_\mp$ if $\alpha=\sigma_\pm$. The application of Eqs. (B3) and (B4) leads in particular to $I^{\sigma_+}_{110}(B_\parallel)=I^{110}_{\sigma_+}(B_\parallel)$ and $I^{\sigma_-}_{110}(B_\parallel)=I^{110}_{\sigma_-}(B_\parallel)$. Since it follows from Eq. (B2) that $I^{110}_{\sigma_-}=I^{1\bar{1}0}_{\sigma_+}$, we finally obtain $\rho^c_{110}(B_\parallel)=\rho^l_{\sigma_+}(B_\parallel)$. For two-step or multistep kinetics, restriction (B3) is lifted and $\rho^c_{110}$ can differ from $\rho^l_{\sigma_+}$.


[1] G. E. Pikus and E. L. Ivchenko, in *Excitons*, edited by E. I. Rashba and M. D. Sturge (North-Holland, Amsterdam, 1982), p. 205.

[2] R. Planel and C. Benoit a la Guillaume, in *Optical Orientation*, edited by F. Meier and B. P. Zakharchenya (North-Holland, Amsterdam, 1984), p. 353.

[3] E. L. Ivchenko, Pure Appl. Chem. **67**, 463 (1995).

[4] E. L. Ivchenko and G. E. Pikus, *Superlattices and Other Heterostructures. Symmetry and Optical Phenomena* (Springer-Verlag, Berlin, 1995).

[5] E. M. Gamarts, E. L. Ivchenko, G. E. Pikus, B. S. Razbirin, V. I. Safarov, and A. N. Starukhin, Fiz. Tverd. Tela (Leningrad) **24**, 2325 (1982) [Sov. Phys. Solid State **24**, 1320 (1982)].

[6] E. Blackwood, M. J. Snelling, R. T. Harley, S. R. Andrews, and C. T. B. Foxon, Phys. Rev. B **50**, 14 246 (1994).

[7] W. A. J. A. van der Poel, A. L. G. J. Severens, and C. T. Foxon, Opt. Commun. **76**, 116 (1990).

[8] C. Gourdon and P. Lavallard, Phys. Rev. B **46**, 4644 (1992).

[9] H. W. van Kesteren, E. C. Cosman, W. A. J. A. van der Poel, and C. T. Foxon, Phys. Rev. B **41**, 5283 (1990).

[10] S. Permogorov, A. Naumov, C. Gourdon, and P. Lavallard, Solid State Commun. **74**, 1057 (1990).

[11] E. L. Ivchenko, V. P. Kochereshko, A. Yu. Naumov, I. N. Uraltsev, and P. Lavallard, Superlattices Microstruct. **10**, 497 (1991).

[12] C. Gourdon, D. Yu. Rodichev, P. Lavallard, G. Bacquet, and R. Planel, J. Phys. IV **3**, 183 (1993).

[13] C. Gourdon, I. V. Mashkov, P. Lavallard, and R. Planel in *Exciton Localization at Normal or Inverted Interfaces in GaAs-AlAs Type II Superlattices*, Proceedings of the 23rd International Conference on the Physics of Semiconductors, Berlin, 1996, edited by M. Scheffler and R. Zimmermann (World Scientific, Singapore, 1997), pp. 1999–2002.

[14] I. L. Aleiner and E. L. Ivchenko, Pis'ma Zh. Eksp. Teor. Fiz. **55**, 662 (1992) [ JETP Lett. **55**, 692 (1992)]; E. L. Ivchenko, A. Yu. Kaminski, and I. L. Aleiner, Zh. Eksp. Teor. Fiz. **104**, 3401 (1993) [JETP **77**, 609 (1993)].

[15] E. L. Ivchenko, A. Yu. Kaminski, and U. Rössler, Phys. Rev. B **54**, 5852 (1996).

[16] S. N. Jasperson and S. E. Shnatterly, Rev. Sci. Instrum. **40**, 761 (1969).

[17] D. Scalbert, J. Cernogora, C. Benoit à la Guilluame, M. Maaref, F. F. Chafdi, and R. Planel, Solid State Commun. **70**, 95 (1989).

[18] P. G. Baranov, I. V. Mashkov, N. G. Romanov, C. Gourdon, P. Lavallard, and R. Planel, Pis'ma Zh. Eksp. Teor. Fiz. **60**, 429 (1994) [JETP Lett. **60**, 445 (1994)].

[19] P. G. Baranov, N. G. Romanov, I. V. Mashkov, G. Khitrova, H. M. Gibbs, and O. Lyngnes, Fiz. Tverd. Tela (Leningrad) **37**, 2991 (1995) [Phys. Solid State **37**, 1648 (1995)].

[20] P. G. Baranov, P. Lavallard, R. Planel, and N. G. Romanov, Superlattices Microstruct. **12**, 327 (1992); N. G. Romanov, P. G. Baranov, I. V. Mashkov, P. Lavallard, and R. Planel, Solid-State Electron. **37**, 911 (1994).

[21] E. L. Ivchenko and A. Yu. Kaminskii, Fiz. Tverd. Tela (Leningrad) **37**, 1418 (1995) [Phys. Solid State **37**, 768 (1995)].